Evolution of the optimal catalytic systems for the oxidative dehydrogenation of ethane: the role of adsorption/desorption in the catalytic performance

Agustín de Arriba [a], Benjamin Solsona [b*], Ana M. Dejoz,[b] Patricia Concepción [a], Narcís Homs [c,d], Pilar Ramírez de la Piscina [c], José M. López Nieto [a*]

[a] *Instituto de Tecnología Química, Universitat Politécnica de València-Consejo Superior de Investigaciones Científicas, Av. Naranjos s/n, 46022 Valencia, Spain*

[b] *Departament d´Enginyeria Química, Universitat de València, C/ Dr. Moliner 50, 46100 Burjassot, Valencia, Spain*

[c] *Departament de Química Inorgànica i Orgànica, Secció de Química Inorgànica & Institut de Nanociència i Nanotecnologia (IN2UB), Universitat de Barcelona, Martí i Franquès 1, 08028 Barcelona, Spain*

[d] *Catalonia Institute for Energy Research (IREC), Jardins de les Dones de Negre 1, 08930 Barcelona, Spain*

* To whom correspondence should be addressed: FAX: +34963877809

Email address: jmlopez@itq.upv.es; benjamin.solsona@uv.es

Abstract:

Three catalysts that correspond to the evolution of the optimal catalytic systems for the oxidative dehydrogenation (ODH) of ethane have been compared in terms of catalytic behavior and adsorption/desorption properties. Thus, the selectivity to ethylene at medium and high ethane conversion during the ethane ODH follows the order: VOx/Al_2O_3 < NiSnOx < MoVTeNb-M1. An opposite trend is observed when comparing the relative reaction rates observed between the oxidation of ethylene and the ODH of ethane (i.e. r_{C2H4}/r_{C2H6}) at 400ºC: VOx/Al_2O_3 < NiSnOx < MoVTeNb-M1. Microcalorimetry and FT-IR of adsorbed ethylene results at low temperature indicate that the heat of adsorption of both ethane and ethylene is the highest in the most selective MoVTeNb-M1 sample. However, operando IR studies of ethylene and O_2 co-adsorption in the 100-250ºC range, clearly indicates a very fast desorption of ethylene on MoVTeNb-M1, whereas O-intermediate compounds and carbons oxides are observed on VOx/Al_2O_3 and NiSnOx. Accordingly, the catalytic results in ethane ODH on these catalysts cannot be directly explained by a weaker adsorption of ethylene at low temperature but to the ability of the catalyst to easily desorb ethylene in the reaction conditions, which favors a low ethylene oxidation and high yield to olefin.

Keywords: ODH ethane; ethylene; FT-IR adsorbed ethylene; microcalorimetry; MoVTeNbO; promoted NiO.

1. INTRODUCTION

It is generally accepted that partial oxidation reactions are carried out by Mars-van Krevelen mechanism [1, 2]. However, other aspects must be also considered such as the possible structure-sensitivity of catalytic reaction on oxides [3], the synergy of catalytic properties in oxide systems, the role of the monolayer in oxide catalysts, the dynamic state of oxide surfaces [4] or the mechanism of catalytic oxidation of hydrocarbons [5]. It is especially remarkable the role of oxygen species in hydrocarbon activation (i.e. electrophilicity and nucleophilicity of oxygen species in oxidation reactions) [3]. In other words: "the surface of a solid is not a rigid static structure, on which various phenomena involving molecules adsorbed from the gas phase occur, but is always in dynamic interaction with the latter" [3]. On the other hand, concepts such as site-isolation and phase cooperation [6], multifunctionality of active sites [7], etc., have subsequently led to postulate the "seven pillars" for the synthesis of oxidation reactions catalysts [8]. These concepts play an important role for the development of efficient catalysts for partial (amm)oxidation of both olefins [2] and alkanes [9].

Oxidative dehydrogenation (ODH) of alkanes is one of the partial oxidation reactions that has received the most attention in the last twenty years, because it could be a more sustainable alternative than the current, non-catalytic, industrial process of olefins production (steam cracking of naphtha, LPG or ethane) [10-12]. Among the different alkanes (C_2-C_4), the ODH of ethane to ethylene is the one that currently generates the best expectations for industrial application [13-17]. From the comparison of the catalytic systems reported in the literature, three different catalysts have been proposed in the last two decades for the ethane ODH, which correspond to the evolution of the most promising catalysts for this reaction [13-17]: i) supported vanadium oxide; ii) promoted nickel

oxide; and iii) multicomponent Mo-V-Te-Nb-O mixed metal oxides (Mo-V-based catalysts presenting orthorhombic molybdenum oxide bronze structure-M1 phase).

In the case of supported vanadium oxide catalysts, it is generally accepted that they should consist of a rather acidic supports, with relatively high interaction of vanadium oxide with the support. This is the case of γ-Al_2O_3-supported vanadium oxide catalysts [18-23], especially those with vanadium loadings not very high (ca. V-loading of 1.4-34.2 V/nm^2), consisting of isolated vanadium species [20] in order to prevent the formation of bulk vanadium pentoxide [18-22]. In the best formulation, vanadia supported on alumina can partially mitigate the ethylene overoxidation when compared to bulk vanadium pentoxide [18, 20, 21].

Promoted-nickel oxide catalysts can be considered as a second group of active and selective catalysts for ethane ODH [24-26]. Nickel oxide alone is not appropriate to get high yields to ethylene because it favors the direct formation of CO_2 from ethane. However, the addition of promoters, especially niobium (with Nb/Ni atomic ratios of ca. 0.03-020) [24], drastically changes the catalytic performance, highly increasing the formation of the olefin at ethane conversions lower than 30%. Apparently, this improvement in the catalytic performance when suitable promoters, such as Nb, Sn, or Ti [24-30], are incorporated is due to the fact that the presence of appropriate metal oxides eliminate electrophilic oxygen species which are highly active in the CO_2 formation. In this way, by keeping nickel in its reduced valence state (Ni^{2+}) and limit the number of O^- radicals that lead to combustion is limited [24, 27, 30, 31]. The main difference between the catalytic performance of undoped and promoted NiO catalysts lies on the extent of the total oxidation of the alkane, rather than to that of the olefin formed. The first step in the mechanism is likely a concerted C-H activation [32] followed by a β-Hydrogen elimination and subsequent release of ethylene and water.

Multicomponent Mo-V-Te(Sb)-Nb-O mixed oxides catalysts consisting in a specific structure (the so-called M1-phase) were reported to show remarkably better behavior than the former vanadium supported catalysts [33, 34]. Their catalytic performance in ethane oxidation can be related to the presence of the multifunctional $Te_2M_{20}O_{57}$ (M= Mo, V, Nb) orthorhombic phase [35-40], in which V-atoms are the active sites (the number of V atoms in pure M1 phase is estimated to be of ca. 1.8×10^{19} V-atoms g_{cat}^{-1} [37]). In addition, the presence of tellurium atoms in the framework of an orthorhombic bronze structure occupying the hexagonal channels, facilitates the modification of acid sites on the catalyst surface preventing the deep oxidation of both ethane and ethylene to carbon oxides [41-42]. These catalysts have been studied for the last years in order to improve catalytic activity [35-42], however, the nature of active/selective species is not completely determined. In this way, it has been proposed that V-sites are the actives ones [35-40], whereas the presence of Te-atoms could favor specific transformation of the catalysts structure, changing the characteristics of active sites and favoring higher selectivity to ethylene [43].

In this paper it is compared the catalytic performance for ethane and ethylene oxidation of representative catalysts of the last three groups, i.e. a multicomponent Mo-V-Te-Nb-O mixed metal oxide (with a Mo/V/Te/Nb atomic ratio of 1.0/0.25/0.17/0.17) [35]; a Sn-doped NiO catalysts (with a Ni/Sn atomic ratio of 92/8) [28]; and a vanadium oxide supported on γ-Al_2O_3 (with 5 wt% of V-atoms) [18]. The role of surface Lewis acid sites in the adsorption enthalpy of ethane and ethylene on the different systems will be studied correlating micro calorimetric with infrared spectroscopy (IR) studies, and the catalytic performance assess by operando IR studies where the reactivity of ethylene in the presence of molecular oxygen will be studied highlighting the role of surface oxygen species in the overoxidation of ethylene.

2. EXPERIMENTAL

2.1. Catalyst preparation

A multicomponent Mo–V–Te–Nb–O catalyst has been prepared hydrothermally from aqueous gels of vanadyl sulfate, niobium oxalate, ammonium heptamolybdate, and telluric acid with a Mo/V/Te/Nb atomic ratio of 1–0.25–0.17–0.17 [35]. The gel was transferred to a Teflon-lined stainless-steel autoclave and kept at 175 ºC/60 h. The resulting precursor was filtered, washed, dried at 100 ºC/16 h, and heat-treated at 600ºC/2h in N_2. This catalyst has been named as MoVTeNb-M1.

Sn-doped nickel oxide catalyst was prepared through the evaporation at 60 ºC of a stirred ethanolic solution of nickel nitrate, $Ni(NO_3)_2.6H_2O$ (Sigma–Aldrich), and tin oxalate, SnC_2O_4 (Sigma– Aldrich) [28]. Oxalic acid has been added to the ethanolic solution with an additive/Ni molar ratio of 1.3 and a Ni/Sn atomic ratio of 92/8 was used. The paste obtained was dried overnight at 120 ºC and finally calcined in static air for 2 h at 500 ºC. This catalyst has been named as NiSnOx.

Vanadium oxide supported on γ-alumina catalyst has been prepared by a wet impregnation method [18]. An ammonium metavanadate (Sigma–Aldrich) aqueous solution was adjusted at pH=7 with diluted nitric acid and to this γ-Al_2O_3 (Suede-Chimie, S_{BET} = 188 m^2 g^{-1}) support was added. The amount of ammonium metavanadate used has been adjusted to fix the vanadium content in 5 wt.% V. This mixture was rotary evaporated using vacuum until a paste was obtained. This paste was dried overnight at 100 ºC and finally calcined in static air for 6 h at 550 ºC. This catalyst has been named as VOx/Al_2O_3. The characteristics of the catalysts are shown in Table 1.

2.2. Catalyst Characterization

The chemical analysis of the solids has been performed by inductively coupled plasma atomic emission spectrometry (ICP-AES).

The specific surface areas have been determined by BET method from N_2 adsorption isotherms at 77 K measured in a *Micromeritics TriStar 3000* instrument.

X-ray diffraction (XRD) patterns of powder solids were collected with a *PANalytical CUBIX* instrument equipped with a graphite monochromator, employing Cu Kα radiation (λ=0.1542 mm) and operated at 45 kV and 4 mA. Distribution of crystalline phases forming the catalysts was calculated by *Rietveld* refinement of the XRD patterns employing *X´Pert Highscore Plus* software.

Raman spectra were recorded with an "in via" Renishaw spectrometer equipped with an Olympus microscope. The samples were excited by the 514.5 nm line of an Ar+ laser (Spectra Physics model 171) with a laser power of 2.5 mW [44] or by the 325 nm (UV-Raman), generated with a Renishaw HPNIR laser with a power of approximately 15 mW [45].

The adsorption enthalpy of hydrocarbons (ethane or ethylene) onto the different catalysts, was measured in separate experiments using a Sensys evo TG-DSC instrument from Setaram, equipped with a 3D thermal flow sensor. The sample (60-100 ± 1 mg) was treated in He flow (50 mL min^{-1}) at 5°C min^{-1} up to 300ºC, kept for 30 min and then cooled down to 35 °C under He flow. After that, a mixture of ethane/He or ethylene/He (10% v/v) was flowed (10 mL min^{-1}) to the catalyst at 35 °C until no variations on mass and heat flow were detected. The exothermic peaks corresponding to the adsorption were integrated to provide the total enthalpy of adsorption. The mean adsorption energy for

each hydrocarbon was calculated by considering the total adsorbed amount of hydrocarbon.

IR spectra of adsorbed CO were recorded at low temperature (-165ºC) with a Bruker Vertex 70 spectrometer using a DTGS detector and acquiring at 4 cm^{-1} resolution. An IR cell allowing in situ treatments in controlled atmospheres and temperatures from -165 ºC to 500 ºC has been connected to a vacuum system with gas dosing facility. For IR studies the samples were pressed into self-supported wafers and treated at 250 ºC in Oxygen flow (10 ml min^{-1}) for 1.5 h followed by evacuation at 10^{-4} mbar at the same temperature for 1h. After activation the samples were cooled down to -165ºC under dynamic vacuum conditions followed by CO dosing at increasing pressure (0.4-8.5 mbar). IR spectra were recorded after each dosage.

In the operando IR experiments, after sample activation under similar conditions as in the IR-CO experiments, 43 mbar ethylene and 84 mbar O_2 were co-adsorbed at 25ºC. Then the temperature was increased stepwise to 100, 150, 200 and 250ºC. IR spectra were recorded after each dosage on the "hot" and "cooled down" pellet.

2.3. Catalytic tests

The catalytic experiments were carried out under steady state conditions using a fixed-bed quartz tubular reactor (i.d. 20 mm, length 400 mm), equipped with a coaxial thermocouple for catalytic bed temperature profiling, working at atmospheric pressure in the 350-450 ºC temperature range. The flow rate (25–100 ml min^{-1}) and the amount of catalyst (0.5–2.0 g, 0.3–0.5 mm particle size) were varied in order to achieve different ethane conversion levels. The feed consisted of a mixture of hydrocarbon/oxygen/helium with molar ratios of 5/5/90 (using ethane or ethylene) or CO/air with molar ratios of 0.5/99.5. Reactants and reaction products were analyzed by on-line gas chromatography,

using two columns [44]: i) Porapak QS (2.0 m × 1/8 in); and ii) (ii) Carbosieve-S (2.5 m × 1/8 in).

3. RESULTS AND DISCUSSION

3.1. Characterization of catalysts

The XRD pattern of multicomponent Mo-V-Te-Nb-O mixed metal oxides catalyst (MoVTeNb-M1) is characterized by the main presence of diffraction peaks related to $(TeO)_2M_{20}O_{56}$ structure [JCPDS: 18-582], the so-called M1 phase [35-41] (Figure S1-A). Moreover, the presence of secondary phase with hexagonal structure, $Te_{0.33}Mo_{0.7}(V/Nb)_{0.3}O_{3.33}$, the so-called M2 phase, as minority, cannot be completely ruled out. The corresponding Raman spectrum, using the 514 nm wavelength excitement laser, showed an intense band at ca. 872 cm^{-1} with a broad shoulder in the 770–840 cm^{-1} region and a signal at 477 cm^{-1}. These signals could correspond to both asymmetric and symmetric stretching modes of the Me-O-Me bonds, respectively (Fig. S1- B). Moreover, it can be also seen a weak shoulder at ca. 980 cm^{-1}, assigned to stretching vibrations of terminal Mo=O and V=O [44] and a band at ca. 664 cm^{-1} that, along with the broad band at ca. 820 cm^{-1} is assigned to the Nb-O-Nb bonds [45]. All these signals confirm the main presence of M1 phase [44]. Furthermore, the XPS of the vanadium $2p_{3/2}$ core level is included in Figure S1-C. A unique symmetrical signal at ca. 515.2 eV is observed, suggesting the single presence of V^{4+} species [35].

SnO_2 –doped NiO catalyst (NiSnOx), with a Ni/Sn at. ratio of 92/8, presents a surface area of 84 $m^2\ g^{-1}$, and a typical X-ray diffraction pattern characterized by the presence of NiO crystallites (JCPDS: 78-0643) with the presence as minority of SnO_2 (JCPDS 41-1445) (Fig. S2-A) [28]. Visible Raman spectra (514 nm) of this catalyst is characterized by the presence of a broad band at ca. 516 cm^{-1}, suggesting some modification of NiO

crystallites [46] (Figure S2-B). In addition, the UV-Raman spectrum (325 nm) of the NiSnOx catalyst confirm the presence of NiO nanoparticles [47], with the presence of five bands which correspond to one-phonon LO modes (at 516 and 580 cm^{-1}), two-phonon 2TO modes (at 707 cm^{-1}), TO + LO (at ~906 cm^{-1}) and 2LO (at ca. 1109 cm^{-1}) modes, respectively. On the other hand, the visible Raman spectrum for this catalyst, present a broad single band at ca. 516 cm^{-1}, as observed in other promoted NiO catalysts [46]. In addition, Figure S2-C shows the Ni $2p_{3/2}$ core level spectrum, in which it can be seen the characteristic peaks for NiO with a main signal at ca. 853.7 eV, along with a broad satellite (Sat II) at ca. 860.9 eV, both associated with Ni^{2+} species, and a second signal (Sat I) at higher binding energy (855.7 eV) than that of the main one, which is related to the presence of defects such as Ni^{3+}, Ni^{2+} vacancies or Ni^{2+}-OH species [28,30].

γ-Al_2O_3-supported vanadium oxide catalyst (VOx/Al_2O_3), with a surface area of 146 m^2 g^{-1}, presents a typical X-ray diffraction patterns of the pure support with no apparent presence of vanadium pentoxide (Fig. S3-A), which suggest that vanadium species are highly dispersed on the surface of the support. This is also confirmed by Raman spectroscopy (Fig. S3-B), which shows a band at ca. 927 cm^{-1} (broad band 920-940 cm-1 in UV Raman) in agreement with a good dispersion of polymeric vanadium species onto the alumina surface [48]. In any case, both UV and visible Raman spectra confirms the absence of V_2O_5 crystallites. In addition to this, XPS analysis of the vanadium $2p_{3/2}$ core level showed an asymmetric signal centered at ca. 516.5 eV (Fig. S3-C), suggesting the main presence of V^{5+} [49]. However, the minority presence of V^{4+} species, with binding energies at 514.5 eV, should be also considered.

Figure 1 presents the TPR patterns of catalysts. For MoVTeNb-M1 sample, a peak at ca. 500ºC and a second peak at ca. 520ºC is observed (the first one related to surface species and the second one related to the reduction of bulk) [50]. However, a single reduction

peak, with the maximum for H_2 consumption at ca. 320ºC and 480 ºC has been observed in the case of NiSnOx and VOx/Al_2O_3 catalysts, respectively, which is in agreement with previous results as seen in [28] and [18]. We must indicate that surface and bulk reduction is observed for MoVTeNb-M1 and NiSnOx catalysts, whereas only the surface vanadium species of the catalyst is reduced in VOx/Al_2O_3.

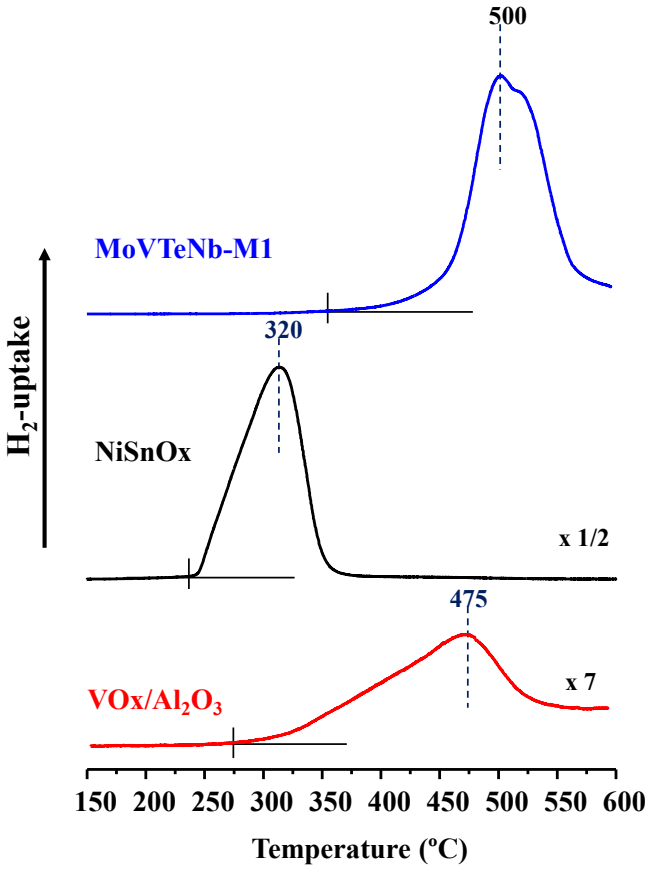

Figure 1. TPR-H_2 results of catalysts: a) MoVTeNb-M1, b) NiSnOx, and c) VOx/Al_2O_3.

The amount of adsorbed hydrocarbons and the heat of adsorption of ethane and ethylene, measured by microcalorimetry are summarized in Table 2. From our calorimetric experiments we can assume that high surface coverage occurs; thus, all adsorption sites, strong and weak are covered. MoVTeNb-M1 shows the highest heat of adsorption, 32 kJ mol^{-1}; with ethylene interacting slightly stronger than ethane, a value of 39 kJ mol^{-1} is

obtained in this case, which is in good agreement to previous results [37]. The adsorption enthalpy of both ethane and ethylene on VOx/Al_2O_3 and NiSnOx catalysts results in low heat values of 10-13 kJ mol^{-1}, which are close to the condensation of the hydrocarbon molecules [37]; there is no apparent strong interaction of these hydrocarbons with the surface of both VOx/Al_2O_3 and NiSnOx catalysts.

The amount of adsorbed hydrocarbon (ethane and ethylene) on MoVTeNb-M1 is about the half than that determined for VOx/Al_2O_3 and NiSnOx catalysts (Table 2). For a more proper comparison of the amount of adsorbed hydrocarbons on the different catalysts, the measured amount was normalized to the specific surface area. The density of active surface sites for the ethane adsorption follows the order: MoVTeNb-M1 (4.9 μmol_{C2H6} m^{-2}) > NiSnOx (1.8 μmol_{C2H6} m^{-2}) > VOx/Al_2O_3 (0.8 μmol_{C2H6} m^{-2}). They are similar to those observed by the ethylene adsorption: MoVTeNb-M1 (5.3 μmol_{C2H4} m^{-2}) > NiSnOx (1.5 μmol_{C2H4} m^{-2}) > VOx/Al_2O_3 (0.8 μmol_{C2H4} m^{-2}). Note that the surface density of sites for ethylene and ethane adsorption is kept in a similar range for each catalyst.

IR spectra of CO adsorption as probe molecule for surface Lewis acid titration performed at -165 ºC shows a density of acid sites in the MoVTeNb-M1 sample higher, than those achieved for NiSnOx and VOx/Al_2O_3, as visualized from the area of the IR signal normalized to catalyst surface area (Fig. 2).

Concerning to the acid strength, it is assumed that a blue shift of the ν(C≡O) corresponds to a higher acid strength, which is the case of the MoVTeNb-M1 sample exhibiting a higher acidity (infrared band at 2175 cm^{-1}) than both NiSnOx (2170 cm^{-1}) and VOx/Al_2O_3 (2157 cm^{-1}). Interestingly, the IR band at 2131 cm^{-1} in the MoVTeNb-M1 sample may be ascribed to reduced Mo and/or V species characterized by π back bonding shifting the IR frequency of C≡O to lower values, while the band at 2144 cm^{-1} could be related to phsysisorbed CO inside the hexagonal channels of the M1 structure [51,52].

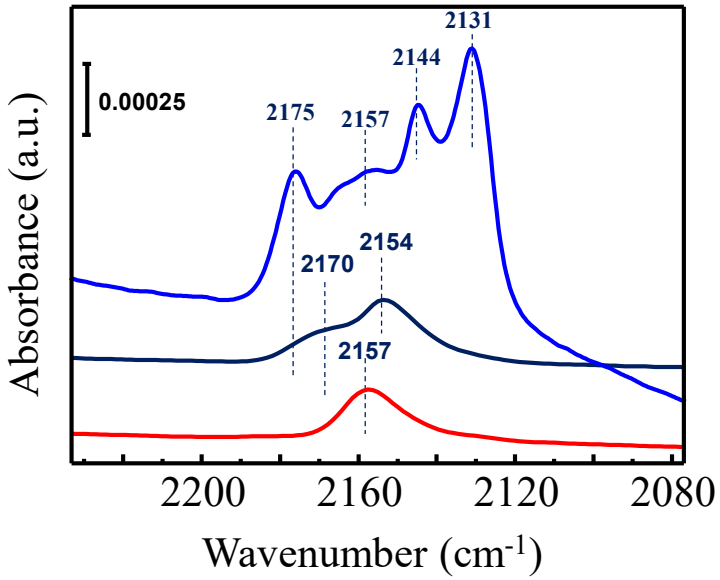

Figure 2. IR spectra of CO adsorption at saturation coverage at -165 ºC on MoVTeNb-M1 (blue), NiSnOx (black) and VOx/Al_2O_3 (red). IR spectra have been normalized to sample weight and surface area.

In order to correlate the strength of surface Lewis acid sites with the previous micro calorimetric studies, IR studies of ethylene adsorption have been performed (Fig. 3). A band in the 1600-1630 cm^{-1} range can be related to the presence of ν(C=C) of ethylene adsorbed in the surface of the catalyst [53]. This band at 1600-1630 cm^{-1} has been observed for all the catalysts, as shown in Figure 3. However, the ν(C=C) of ethylene is red shifted in the MoVTeNb-M1 sample (IR band at 1604 cm^{-1}) compared to that of the NiSnOx (~1629 cm^{-1}) and VOx/Al_2O_3 (~1629 cm^{-1}) samples, indicating a higher interaction strength between the olefin group and the Lewis acid site in the MoVTeNb-M1 sample, in agreement with the higher heat of adsorption determined by microcalorimetry.

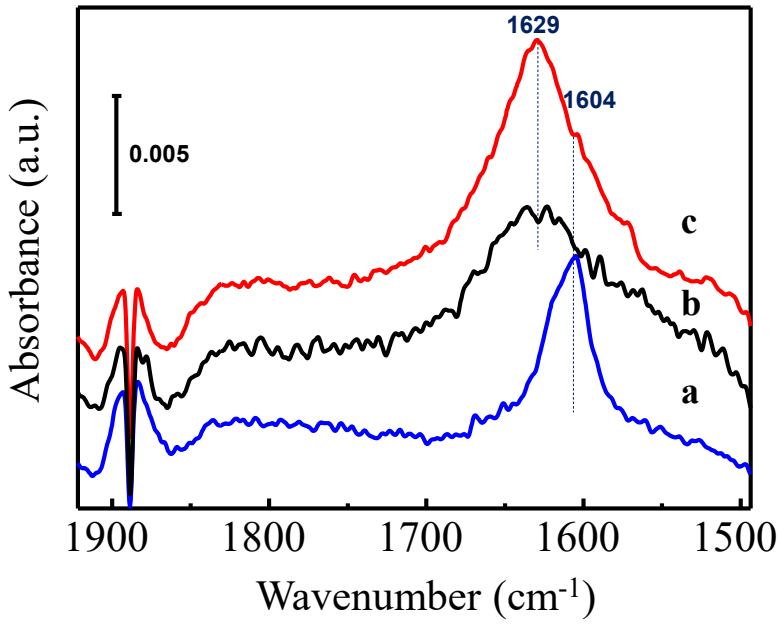

Figure 3. IR spectra of 43 mbar of ethylene adsorbed at 25 ºC on MoVTeNb-M1 (blue), NiSnOx (black) and VOx/Al_2O_3 (red). IR band in the 1600-1630 cm^{-1} range corresponds to the ν(C=C).

3.3 Catalytic results

The catalytic performance of these catalysts (i.e. MoVTeNb-M1, NiSnOx and VOx/Al_2O_3) in the oxidative dehydrogenation (ODH) of ethane and in the oxidation of ethylene has been comparatively studied at a fixed and relatively low reaction temperature (in the 350-450ºC temperature range), maintaining the same Hydrocarbon/O_2/He = 5/5/90 molar ratio and modifying the contact time by changing the catalyst weight and/or the total flow. This way we can observe the evolution of the selectivity to the main reaction products when the ethane conversion increases. A summary of the catalytic results in the ODH of ethane on these catalysts is shown in Table 3. We must note that other experiments were undertaken using different reactant concentrations in order to determine the reaction orders referred to oxygen and to hydrocarbon.

The reactivity of the multicomponent Mo-V-Te-Nb-O mixed metal oxides catalysts, presenting mainly M1, is likely only due to the reactivity of the vanadium sites in a suitable environment [33-43]. In fact, it is known that molybdenum oxide-based catalysts can activate ethane at temperatures over 500ºC [19], which are much higher than the reaction temperature of the present work; whereas tellurium and niobium sites are inert in these reaction conditions. The reaction rate of ethane transformation per mass of catalyst ($\mathbf{r}_{C2H6}$) is 2.29 $mmol_{C2H6}\ g_{cat}^{-1}\ h^{-1}$, whereas the rate per mass of active site (vanadium) is 60.3 $mmol_{C2H6}\ g_{V}^{-1}\ h^{-1}$.

The reactivity of VOx/Al_2O_3 catalyst is due to the vanadium sites and depends on both the reducibility of catalyst and the subsequent reoxidation of reduced catalysts [20, 54], since at the reaction temperature used in this work, the reactivity of pure γ-Al_2O_3 has been shown as negligible. The reaction rate of ethane transformation per mass of catalyst ($\mathbf{r}_{C2H6}$) is 0.424 $mmol_{C2H6}\ g_{cat}^{-1}\ h^{-1}$ (Table 2), whereas the rate per mass of active site (vanadium) is ca. 13.7 $mmol_{C2H6}\ g_{V}^{-1}\ h^{-1}$.

The reactivity of NiSnOx catalyst is due to the nickel sites [24-30], as the tin sites are inactive in the ethane activation in these reaction conditions [28]. Thus, in this case, the reaction rate of ethane transformation per mass of catalyst ($\mathbf{r}_{C2H6}$) is 17.6 $mmol_{C2H6}\ g_{cat}^{-1}\ h^{-1}$ whereas the rate per mass of active site (nickel) is 26.3 $mmol_{C2H6}\ g_{Ni}^{-1}\ h^{-1}$.

Accordingly, the reaction rate for ethane oxidation ($\mathbf{r}_{C2H6}$) during the ethane ODH at 400ºC decreases according to the following trend: NiSnOx (17.6 $mmol_{C2H6}\ g_{cat}\ h^{-1}$) > MoVTeNb-M1 (2.29 $mmol_{C2H6}\ g_{cat}\ h^{-1}$) > VOx/Al_2O_3 (0.68 $mmol_{C2H6}\ g_{cat}\ h^{-1}$) (Table 3).

Figure 4 shows the variation of the selectivity to ethylene with the ethane conversion at 400ºC (data obtained varying the contact time). By comparing the variation of the selectivity to ethylene with ethane conversion at 400ºC it can be concluded that ethane conversion has a very low influence on the selectivity to ethylene when the reaction is

carried out over multicomponent MoVTeNb-M1 catalysts, with selectivity to ethylene higher than 90% for ethane conversion up to 80%. However, a higher influence of ethane conversion on the selectivity to ethylene is observed for NiSnOx, and especially for VOx/Al_2O_3 catalyst (Fig. 4).

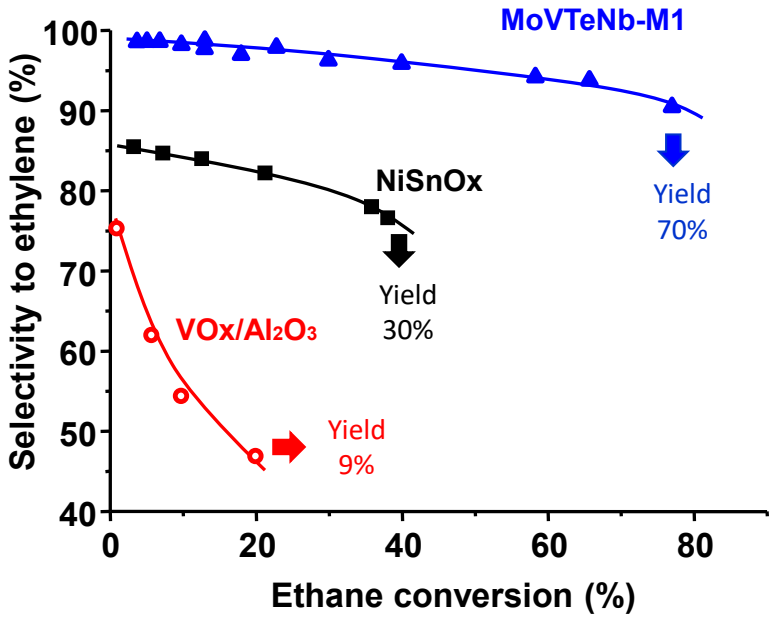

Figure 4. Variation of the selectivity to ethylene with the ethane conversion at 400 °C in the ODH of ethane. Catalysts: MoVTeNb-M1 (▲), NiSnOx (■), VOx/Al_2O_3 (●). Remaining reaction conditions in text. Detailed data of representative catalysts are shown in Table S1.

In the ODH of ethane on multicomponent MoVTeNb-M1 catalyst three reaction products have been observed: ethylene (mainly), and CO and CO_2 as minority (whereas acetic acid was not observed) (Table S1). Initially, the ethane is transformed into ethylene as its initial selectivity to ethylene is ca. 100% (Fig. 4). Interestingly, the selectivity to ethylene hardly decreases with the ethane conversion (from 99% at 2% ethane conversion to 96% at 40% ethane conversion). In addition, no influence of reaction temperature on selectivity to ethylene is observed on this catalyst in the 350-450ºC range (Fig. S4).

In an opposite trend, a drastic decrease of the selectivity to ethylene is observed on VOx/Al_2O_3 catalyst when the ethane conversion increases. Thus, VOx/Al_2O_3 catalyst presents an initial selectivity to ethylene of ca. 80% (at 400ºC) or 90% at (450ºC), whereas both CO (initial selectivity of ca. 16% or 6%, at 400 or 450ºC, respectively) and CO_2 (initial selectivity ca. 4% regardless of the reaction temperature) can be also directly formed from ethane (Figure S4).

It is noteworthy to mention the selectivity achieved over the alumina-supported vanadium oxide catalyst presented here is even lower compared to other vanadia/alumina catalysts reported in the literature [20, 54]. However, this is related to the low reaction temperature used in the present study in contrast with typical reaction temperatures of 500-550ºC reported elsewhere [18-20], and the strong influence of reaction temperature on selectivity to ethylene [20], in part as a consequence of the reducibility and re-oxidation of the catalyst [54].

An intermediate behavior is observed over the Sn-doped NiO catalysts (NiSnOx). Most of ethane is transformed into the olefin, with an initial selectivity to ethylene of 85-90% being achieved (Fig. 4). However, a slight decrease of the selectivity to ethylene is observed when the ethane conversion increases (from 86% at 2% ethane conversion to 76% at 40% ethane conversion), but a greater influence of the ethane conversion on the selectivity to ethylene is observed for higher ethane conversion. In addition, we must inform that only two reaction products (ethylene and CO_2) have been observed during the ODH of ethane over NiSnOx catalyst. Nevertheless, no influence of reaction temperature on selectivity to ethylene is observed between 400 and 450ºC (Fig. S4).

On the other hand, the catalysts have been tested in the oxidation of ethylene (Table S2, supplementary information) and the selectivity to the main reaction products is presented in Figure 5.

In the oxidation of ethylene over MoVTeNb-M1 or VOx/Al_2O_3 catalyst two reaction products (CO and CO_2) have been observed (Fig. 5 and Table S2), although acetic acid was also detected, as traces, over VOx/Al_2O_3. In both cases, the selectivity to carbon oxides kept constant with the ethylene conversion, suggesting that there has not been an appreciable CO oxidation into CO_2. However, only CO_2 was identified during the ethylene oxidation over NiSnOx catalyst (Fig. 4): neither CO nor acetic acid were detected.

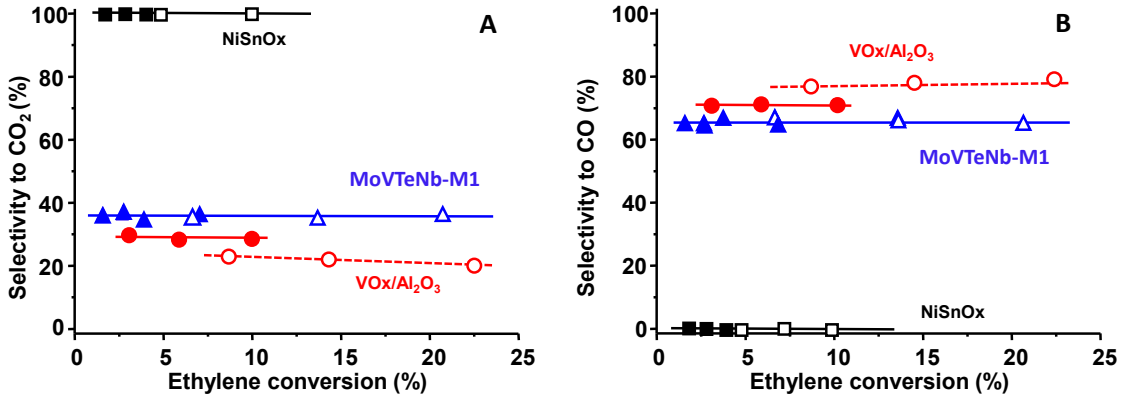

Figure 5. Variation of the selectivity to CO and CO_2 with the ethylene conversion, at 400 (●,▲, ■) and 450ºC (○, Δ, □,), during the oxidation of ethylene over MoVTeNb-M1 (▲, Δ), NiSnOx (■, □) and VOx/Al_2O_3 (●, ○) catalysts. Reaction conditions in the experimental section.

The reaction rate of ethylene transformation per mass of catalyst during the ethylene oxidation at 400ºC ($\mathbf{r}_{C2H4}$) decreased according to the following trend: NiSnOx (3.71 $mmol_{C2H6}\ g_{cat}^{-1}\ h^{-1}$) > VOx/Al_2O_3 (1.76 $mmol_{C2H4}\ g_{cat}^{-1}\ h^{-1}$) > MoVTeNb-M1 (0.166 $mmol_{C2H6}\ g_{cat}^{-1}\ h^{-1}$).

Figure 6 shows the variation of ethane or ethylene conversion with the contact time during their oxidation over MoVTeNb-M1 (Fig. 6a), NiSnOx (Fig. 6b) and VOx/Al_2O_3 (Fig. 6c)

catalysts at 400ºC. The corresponding r_{C2H4}/r_{C2H6} ratios achieved for each catalytic system have been also included. These reaction rates have been calculated considering hydrocarbon conversions lower than 5 %.

The reactivity of MoVTeNb-M1 catalyst in the olefin transformation resulted to be ca. 15 times lower than that in the ethane transformation (Fig. 6a), which is in agreement with the extremely low drop in the selectivity to ethylene observed during the ODH of ethane (Fig. 4). On the other hand, NiSnOx catalyst in the ethylene transformation resulted to be low, only around 1/5 of the reaction rate observed in the alkane transformation (Fig. 6b), which can explain the slow drop in the selectivity to ethylene observed during the ODH of ethane (Fig. 4). However, in the case of VOx/Al_2O_3 catalyst, its catalytic activity in the ethylene transformation resulted to be 2-3 times higher than that in the ethane transformation (Fig. 6c), which is in agreement with the important drop in the selectivity to ethylene observed during the ODH of ethane (Fig. 4).

Furthermore, in previous comparative studies of undoped and Zr- or Nb-doped NiO catalysts for ethane ODH at 350ºC, it was observed that the r_{C2H4}/r_{C2H6} ratio shows small differences between 0.41-0.53 [55], similar to that reported here. However, supported vanadium oxide catalysts present r_{C2H4}/r_{C2H6} ratios between 2 to 10, depending on the hydrocarbon feed and the support [16].

The results presented here clearly explain the higher selectivity to ethylene achieved during the ODH of ethane over MoVTeNb-M1 catalysts, and the lower selectivity to ethylene achieved during the ODH of ethane over VOx/Al_2O_3 catalyst, whereas Me-doped nickel oxide catalysts present intermediate selectivity to ethylene. Accordingly, for ethane ODH, the selectivity to ethylene on these catalysts strongly depends on the relative reaction rate for ethane and ethylene oxidation.

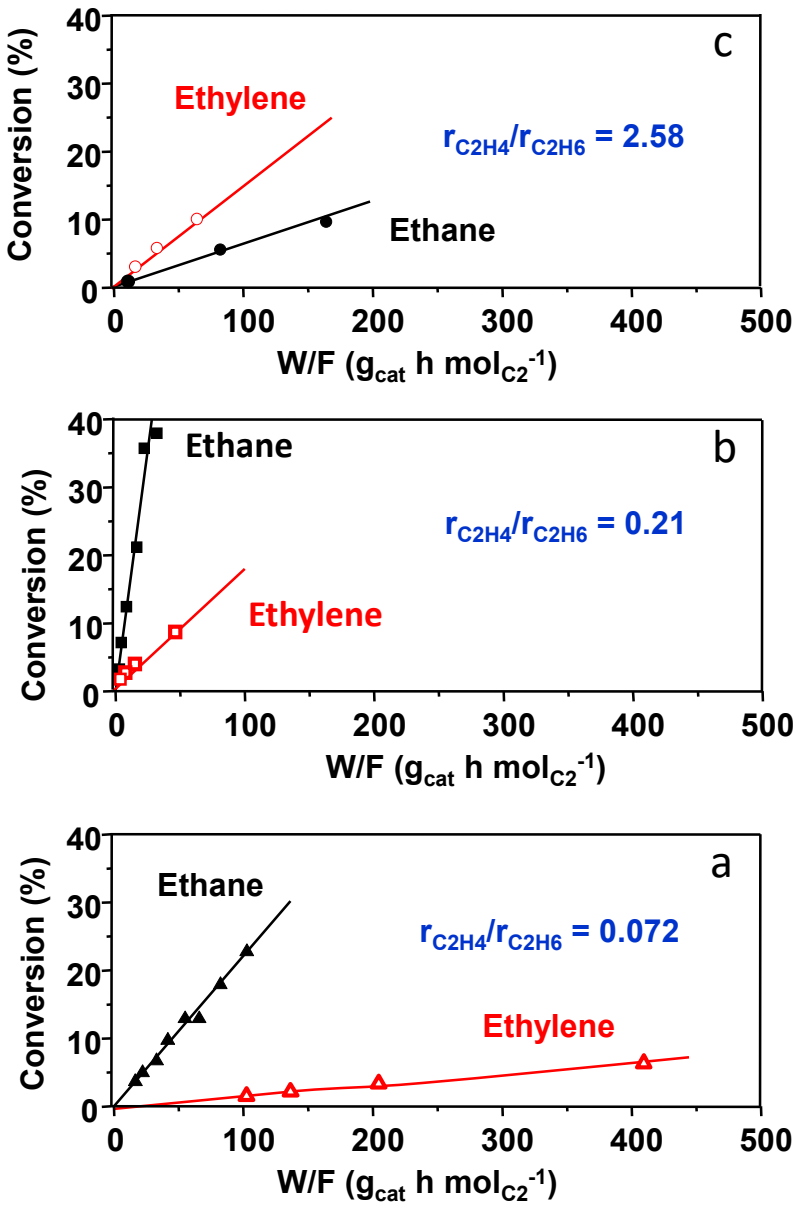

Figure 6. Variation of the ethane and ethylene conversion with contact time, W/F, during the oxidation of ethane and ethylene over MoVTeNb-M1 (a), NiSnOx (b) and VOx/Al_2O_3 (c) catalysts. Reaction conditions: 400ºC, C_2/O_2/He: 5/5/90 molar ratio (for ethane or ethylene).

Further experiments undertaken in the oxidation of CO (Figure 7) showed that at the temperature of this study carbon monoxide was hardly transformed into carbon dioxide over MoVTeNb-M1 and VOx/Al_2O_3 catalysts, which is in agreement with the null CO oxidation observed in the ethylene oxidation.

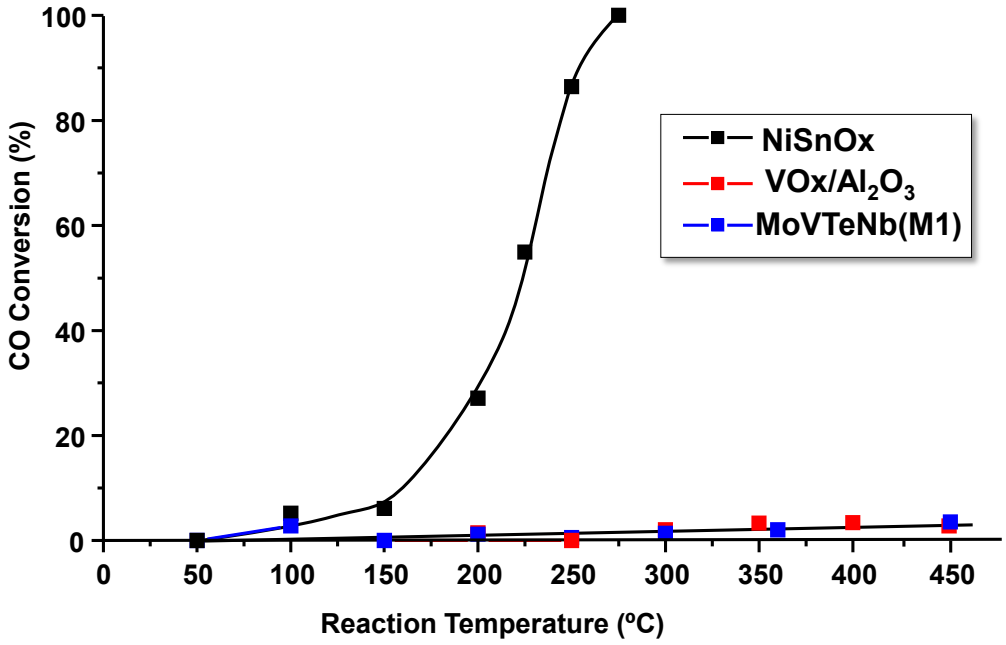

Figure 7. Variation of the Oxidation of CO with reaction temperature over MoVTeNb-M1, NiSnOx and VOx/Al_2O_3 catalysts. Reaction conditions: 0.5 mol% CO in synthetic air; 0.1 g of catalyst; total flow of 50 ml min^{-1}.

However, total conversion of CO into CO_2 was observed at the temperature of this study over NiSnOx catalyst (Fig. 7). Even more, at temperatures of ca. 125ºC below the reaction temperature of this study, the CO conversion had already reached 100%. This is in agreement with the no observation of CO in both ethane and ethylene oxidation reaction over NiSnOx catalyst, as CO quickly transforms into CO_2. These results are in agreement to those previously reported in which the catalytic activity for CO oxidation can be explained by the capability to show homomolecular exchange of oxygen, which strongly depends on the presence/absence and strength of Me=O bond [56]. In this way, undoped and Sn-doped NiO catalysts present rates of homomolecular exchange of oxygen [28] higher to those achieved for MoVTeNbO [44] or supported vanadium oxide [57]

catalysts. However, there is no parallelism between the catalytic activity of each catalyst for CO oxidation (Fig. 7) and the selectivity to ethylene during the ethane ODH (Fig. 4).

According to these catalytic results a general pathway can be proposed in the ODH of ethane on both MoVTeNb-M1 and VOx/Al_2O_3 catalysts (Scheme 1a), although values of kinetic constants strongly depend on the characteristics of catalysts.

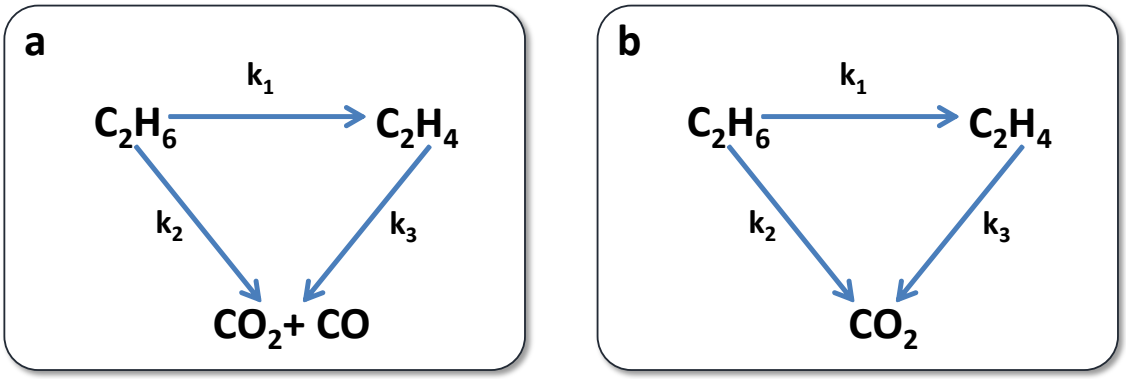

Scheme 1. Reaction scheme for the oxidative dehydrogenation of ethane on: a) MoVTeNb-M1 or VOx/Al_2O_3 catalysts; b) on NiSnOx.

Ethane is initially transformed into ethylene (mainly), CO and CO_2. In addition, the ethylene formed is slowly (MoVTeNb-M1 catalyst) or fastly (VOx/Al_2O_3 catalyst) oxidized into CO (mainly) and CO_2, whereas the CO formed does not transform into CO_2.

On the other hand, a slightly different pathway can be proposed in the ODH of ethane on NiSnOx catalyst (Scheme 1b). Ethane is directly transformed into ethylene (mainly) and CO_2 whereas the ethylene formed oxidizes into CO_2. In spite of the no detection of CO, the appearance of CO as a reaction intermediate in the CO_2 formation is highly likely.

3.4 Infrared study of adsorbed ethylene

In order to obtain fundamental knowledge of the processes taken place on the catalyst surface, operando IR studies of ethylene and O_2 co-adsorption have been performed at increasing reaction temperatures from 25ºC to 250ºC (Figs. 8 and 9).

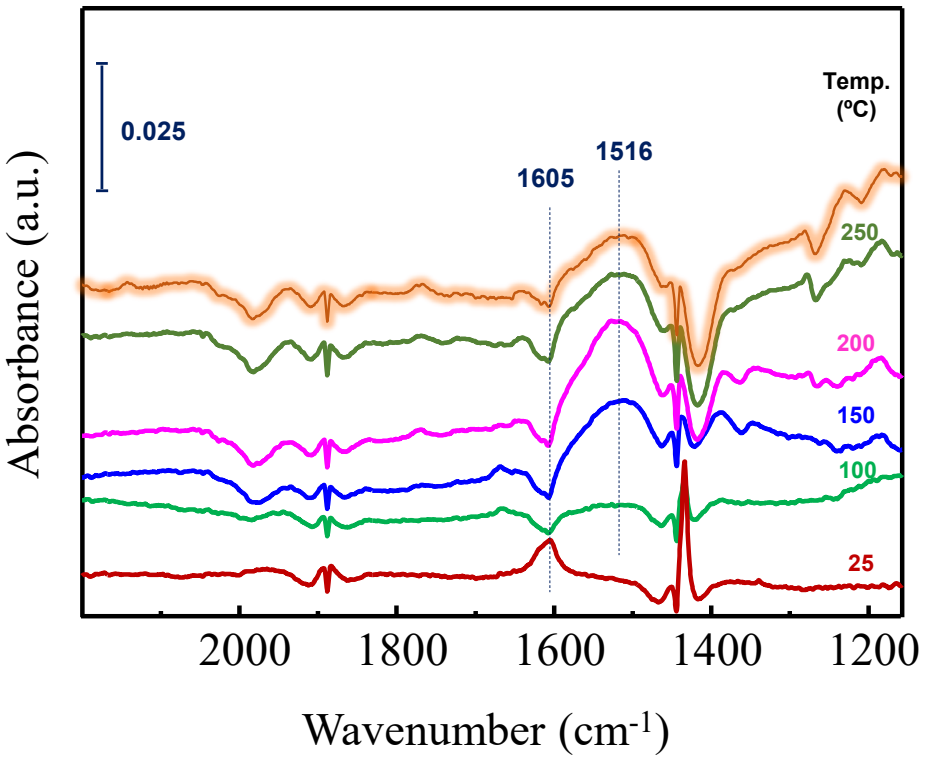

Figure 8. IR spectra of the co-adsorption of ethylene and O_2 on MoVTeNb-M1 catalyst at increasing reaction temperatures: 25 ºC (red); 100 ºC (green); 150 ºC (blue); 200ºC (magenta); 250 ºC light grey (dark green). Cooling down to 25 ºC (highlighted orange line).

In the MoVTeNb-M1 sample (Figure 8) a fast desorption of ethylene is observed at 100ºC (depletion of the IR band at 1605 cm^{-1}), followed by the absence of additional IR signal at increasing temperature, except for a broad band at 1516 cm^{-1} due to carboxylate species, indicating the practically nonexistence of surface catalyzed reaction between

ethylene and oxygen, in agreement with the high selectivity of this catalyst in the ODH of ethane. After cooling down the IR sample from 250 ºC to 25 ºC, no changes in the spectrum is observed, indicating the absence of reaction during the experiment.

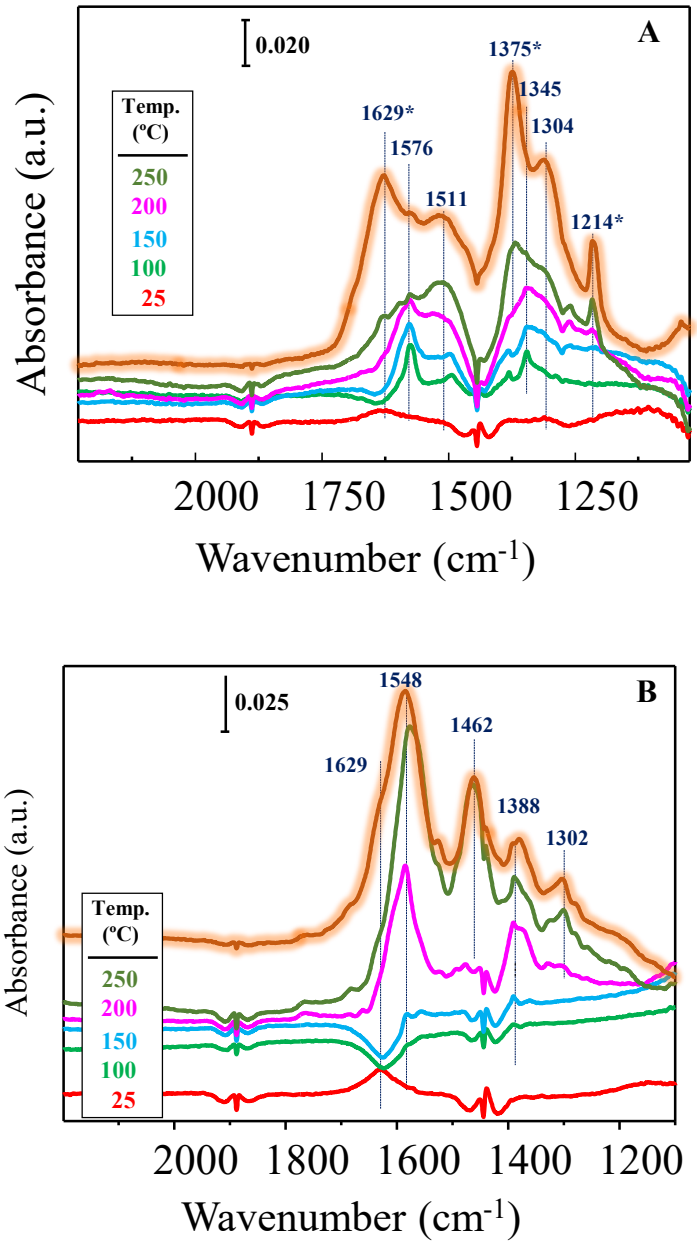

Figure 9. IR spectra of the co-adsorption of ethylene and O_2 on NiSnOx (A) or VOx/Al_2O_3 (B) at increasing reaction temperatures: 25 ºC (red); 100 ºC (green); 150 ºC (blue); 200ºC (magenta); 250 ºC light grey (dark green). Cooling down to 25 ºC (highlighted orange line). In asterisk bands due to re-adsorption of ethylene.

In the NiSnOx sample (Fig. 9A), ethylene is desorbed at 100ºC and new IR bands appear at 1576, 1511, 1345 and 1304 cm^{-1} associated to carbonate /carboxylate species, growing in intensity when increasing the temperature. This means a high reactivity of oxygen species resulting in the formation of oxygenated species, precursors of CO_x. Interestingly, after cooling down the IR sample from 250 ºC to 25 ºC, re-adsorption of non-reacted ethylene (IR bands at 1629, 1375 and 1214 cm^{-1}) [58] is observed, indicating the existence of free Lewis sites not involved in the overoxidation reaction.

Finally, in the VOx/Al_2O_3 sample (Fig. 9B), ethylene is desorbed at 100ºC, and until 200ºC no new IR bands are observed. The new bands, which appears at 1584, 1388 cm^{-1}, together with bands at 1462 and 1302 cm^{-1}, formed at 250 ºC, are all of them due to carbonate species. In contrast with the previous sample, re-adsorption of ethylene on the cooled sample is markedly lower, visualized by a small shoulder at 1629 cm^{-1}, indicating that almost all sites are involved in the oxidation path.

This fact may explain the drastic decrease of the selectivity to ethylene observed on the VOx/Al_2O_3 sample when the ethane conversion increases, while this behavior is not observed in the NiSnOx sample. In this last case, the coexistence of free Lewis sites not involved in the oxidation process, may favor the ethane dehydrogenation path.

Interestingly, the different IR patterns observed in the different samples, which should be related to the reactivity of surface oxygen species, agree with the TPR data. Then, the reducibility of active sites is higher in the NiSnOx sample (reduction temperature at 350 ºC), compared to VOx/Al_2O_3 (reduction temperature 480 ºC) and finally MoVTeNb-M1 (reduction temperature 520 ºC). In fact, a Mars van Krevelen mechanism is assumed for these types of catalysts, where lattice oxygen participating in the reaction is replenished by molecular oxygen species. In conclusion, based on our study, the controlling step

dictating the selectivity to ethylene can be ascribed to the reactivity of surface oxygen species in each catalyst.

4. General remarks

In order to explain the catalytic behavior of the studied catalysts, it would be necessary to consider not only the crystalline structure of the material but also the nature and characteristics of the active centers and the influence of the environment of these active center on the selectivity of the studied reaction. Thus, the reducibility of the active center, the reactivity of oxygen species on the catalyst surface and the adsorption/desorption capacity of reactants and products on the catalyst surface are key aspects to define the catalytic behavior of a catalyst [1-9].

It is generally accepted that the selectivity to the main reaction products during the ethane ODH can be explained by considering a simplified reaction network, with parallel and consecutive reactions (Scheme 1a and 1b, in which k_1, k_2 and k_3 are kinetic constants) [13-18]. The initial selectivity to ethylene (at low conversion of alkane) is related to the k_1/k_2 ratio while the selectivity to ethylene at high ethane conversions can be related to the $k_1/(k_2+k_3)$ ratio. According to the catalytic results during the ethane and ethylene oxidation (Figs. 4 to 6), important differences among catalysts can be concluded: i) differences in the nature of deep oxidation products; ii) the different k_2/k_1 ratio for catalysts.

One important difference between NiO-based catalysts and V-containing catalysts is related to the nature of deep oxidation products during ethane or ethylene oxidation (Fig. 5): CO_2 for NiO-containing catalyst, and CO/CO_2 for V-containing catalysts. This behavior can be explained by considering the catalytic performance of these catalysts

during oxidation of CO (Fig. 7). But, in addition, the results of Figure 7 suggest that the capability of a catalyst for CO oxidation is not a key factor for developing selective catalysts for ethane ODH. In fact unpromoted NiO and promoted-NiO catalysts are both very effective in CO oxidation [24-30], whereas their catalytic performance in ethane ODH is completely different. In the case of V-containing catalysts, strong differences in the selectivity to ethylene from ethane depending on the support, vanadia content and preparation method have been reported, presenting in all cases both CO and CO_2 as deep oxidation products [17-21, 33-40]. Therefore, there is not a clear parallelism between the CO/CO_2 ratio and the selectivity to ethylene during the ethane ODH.

Thus, it was proposed a classification of catalysts for C_3-C_4 olefin oxidation according to the type of metal-oxygen bond and their behavior for CO oxidation [61]. However, this classification cannot be completely considered for neither ethylene oxidation nor ethane ODH.

On the other hand, the three catalysts present strong differences in the relative reaction rate in ethylene oxidation and in ethane ODH (i.e. r_{C2H4}/r_{C2H6} ratios in Fig. 6). Thus the r_{C2H4}/r_{C2H6} ratio decreases as: VOx/Al_2O_3 (2.58) > NiSnOx (0.21) > MoVTeNb-M1 (0.072); which explain the differences in selectivity to ethylene at high ethane conversions, during ODH of ethane, and which would determine the strong dissimilarities in the k_2/k_3 ratios in Scheme 1. These variations among catalysts are probably due to significant differences in their physical-chemical properties.

Regarding the nature of these catalysts (promoted and/or supported materials), V-sites or Ni-sites can be proposed as the active sites for ethane ODH. In each case the presence of dopant and/or support strongly modifies the performance of the corresponding pure metal oxide, i.e. NiO [26-30], V_2O_5 [16, 17] or MoO_3 [14, 16, 17]. This is due to the modifications of active sites providing lattice oxygen species for hydrogen abstraction

from ethane [19, 21, 26, 28, 44], which leads to the presence of a higher/lower concentration of nucleophilic oxygen species depending on the catalytic system.

In the case of the Sn-doped NiO catalyst, the presence of the dopant modifies the nature of the active centers (as shown by XPS) by increasing the concentration of nucleophilic oxygen species (according to the $^{18}O_2$ isotopic exchange results [28]), in the same way as those proposed in NiO catalysts doped with niobium [26, 27].

In the case of the VOx/Al_2O_3 catalyst, the support modifies the characteristics of the active sites, favoring the presence of tetragonal VO_4 species less reactive than the vanadium species in V_2O_5 [18-22], and also favoring changes in the nature of the oxygen species [57]. However, the high concentration of V^{5+} species (determined by XPS) favors both the activation of ethane and ethylene on the same active centers [18-21], resulting in a lower selectivity to ethylene at high ethane conversions. In this sense, it has been observed that an initial decrease in V^{5+} species (by treatment with H_2) favors an increase in ethylene selectivity [21]. In this way, it has been recently proposed that Al_2O_3-Supported W–V–O bronze catalysts [62], presenting isolated octahedral V-species, but with higher V^{4+}/V^{5+} concentration than those observed for conventional supported vanadium oxide catalysts, seem to be among the most active and selective catalysts for ethane ODH on supported vanadium oxide catalysts.

In the case of the MoVTeNb-M1 catalyst, its crystalline structure corresponds to a Mo-based orthorhombic bronze (the so-called M1). In catalytic terms, this catalyst can be considered as a monolayer with the active centers on the catalyst surface (in the ab plane), which are not strictly a part of the M1 crystal structure [63]. In other words, the M1 phase would be the support that enables the formation of a thin active surface layer that contains V^{4+}/V^{5+} in close vicinity to Te^{4+} oxo-sites [63]. In addition, the presence of Nb atoms in

optimized catalysts [33-40] can be related to the elimination of Brönsted sites after the incorporation of Nb^{5+} in the framework of the catalyst [41].

In this way, it is observed that during the ethane ODH, MoVTeNbO catalysts are more selective to ethylene at high ethane conversions than MoVTeO [44] or MoVO [40] catalysts. The concentration of nucleophilic oxygen species in MoVTeNbO-based catalysts are higher than those in Nb-free MoVTeO catalysts [44]. Therefore, in some way, we can describe MoVTeNb-M1 catalysts as a surface of Mo-V-Te-Nb-O mixed metal oxide on the crystalline M1 phase, in which the reaction conditions could modify the nature of the surface species, especially V-sites [37, 63].

Accordingly, the presence of a promoter (in Sn-doped NiO catalyst), a support (in alumina-supported vanadium oxide catalyst), or both (in the case of MoVTeNb-M1 catalyst) exerts a positive role in selectivity to ethylene during ODH of ethane, by modifying the reducibility of the active centers and the nature of the surface oxygen species (favoring an increase in nucleophilic species with respect to pure metal oxides). However, there is an additional aspect regarding the MoVTeNbO-M1 catalyst that is not seen in the other catalysts. This catalyst contains heptagonal channels (a 7-membered channel is a micropore with a diameter of ca. 0.4 nm) in which gases smaller than or equal to ethane can enter [36]. In fact, and especially for Mo-V-O materials with structure M1 [36, 62, 63], they have the ability to incorporate ethane and/or ethylene inside the heptagonal channels of the M1 phase.

Thus, the existence of microporosity in M1 phase [37, 64, 65] could explain the results of microcalorimetry (achieved at low temperature and high partial pressures of hydrocarbon), in which an adsorption energy for the MoVTeNb-M1 higher than those observed for the other two catalysts is observed. However, it seems unlikely that this confining effect of ethane or ethylene in the pores of the catalyst is carried out at

temperatures of 350-400ºC (temperatures used in the oxidation reactions of ethane and ethylene), especially considering the molecules moving along the micropores. In fact, the catalytic results suggest that the activity and selectivity to ethylene during the ODH of ethane is more related to the activation of ethane at the entrance of the pores rather than along the micropores.

In this way, the infrared results of CO or ethylene at low temperature (Fig. 2 and 3) suggest a greater and stronger adsorption in the case of the MoVTeNb-M1 catalyst, which could be explained by a certain confinement effect of the molecules within the heptagonal channels. This does not occur in the other two catalysts.

Relationship between adsorption and reactivity is difficult to establish, provided that additional parameters, such as the reactivity of surface oxygen species, play an important role in olefin over-oxidation and accordingly decreases the selectivity in the ODH reaction. However, operando IR studies (Figs. 8 and 9) and TPR-H_2 data (Fig. 1) showed a correlation between catalyst reducibility (i.e. M-O bond strength) and ethylene over-oxidation asses in the IR work. In this case, a fast overoxidation is observed in the NiSnOx sample, exhibiting the lowest reduction temperature in the TPR pattern (320 ºC), followed by the VOx/Al_2O_3 sample (480 ºC), while no over-oxidation is observed in the MoVTeNb-M1, which is the catalyst that presented the highest reduction temperature (520 ºC). By analyzing the catalytic data for ethane ODH, a drastic decrease in the selectivity to ethylene is observed on VOx/Al_2O_3 catalyst compared to NiSnOx, when the ethane conversion increases, while a rather constant selectivity is observed in the MoVTeNb-M1 sample.

We must inform that while a higher over-oxidation ability is observed in the NiSnOx sample versus VOx/Al_2O_3, uncovered surface sites are observed in the NiSnOx sample, as determined in the cooling down experiments (Fig. 9A), favoring the selective

dehydrogenation path, and resulting in a lower extension of ethylene deep oxidation compared to that observed on VOx/Al_2O_3 catalyst (Fig. 9B).

Notoriously, and based on IR results of ethylene and oxygen co-adsorption, it can be concluded that a fast desorption of ethylene occurs on MoVTeNb-M1 catalyst (Fig. 8), without the formation of O-intermediates, during ethylene oxidation. However, O-intermediate compounds and carbon oxides, adsorbed on the surface of catalysts, are clearly observed on both VOx/Al_2O_3 and NiSnOx (Fig.9). Accordingly, the catalytic results in ethane ODH on these catalysts cannot be directly explained by a weaker adsorption of ethylene at low temperature but to the ability of the catalyst to easily desorb ethylene in the reaction conditions, which favors a low ethylene oxidation and high yield to the olefin.

According to the density functional theory (DFT) analysis for ethane ODH over M1 phase MoVTeNbO mixed oxides, it has been proposed that the high selectivity to C_2H_4 requires O atoms inside the pores, with low tendency to form C-O bonds [66]. Our IR results of ethylene and oxygen co-adsorption confirm that MoVTeNbO based catalyst has a very low ability to form O-intermediates from ethylene (with very low reactive vinylic H atoms [14, 17]) (Fig. 8), and ethylene is easily desorbed at temperatures near to those used in oxidation reactions. However, O-intermediates (and carbon oxides) adsorbed on the surface of catalysts have been observed after co-adsorption of ethylene and oxygen when using Sn-doped NiO and alumina-supported vanadium oxide catalysts (Fig. 9).

The low reactivity of ethylene over MoVTeNb mixed oxide catalyst during ethane oxidation contrast with the behavior observed on the same catalysts during the selective propane oxidation [6, 7, 67-69], since propylene readily converts into O-containing compounds. In fact, in the last case, the olefin (C_3H_6 with allylic H atoms) can be easily transformed in Te-containing entities on the surface of the catalyst to form a π-allylic

compound [67], intermediate in the selective oxidation of propylene to acrylic acid [6, 7, 66-69].

5. Conclusions

The different catalytic performance of the three most significant catalysts reported during the last decades for the oxidative dehydrogenation of ethane to ethylene (i.e. MoVTeNbO mixed metal oxides, Sn-doped NiO and Al_2O_3-supported vanadium oxide) has been comparatively studied. This work reports that the differences in the catalytic performance in ethane ODH of these catalysts can be related to the strong differences between the ethane and ethene oxidation over these catalysts and, especially, to the variable extent of the ethylene oxidation. In this sense, the over-oxidation of ethylene is the highest for the VOx/Al_2O_3 catalyst and the lowest for MoVTeNb-M1, with NiSnOx catalyst presenting an intermediate behavior. In addition, when considering the reaction rates for ethane and ethylene oxidation, a reactivity for ethane oxidation more than 10 times higher than that for ethylene oxidation (i.e. r_{C2H4}/r_{C2H6} ratio is 0.072 at 400ºC) is observed over MoVTeNb-M1 catalyst. This contrasts with the other catalysts with r_{C2H4}/r_{C2H6} ratios of 0.21 (NiSnOx) or 2.58 (VOx/Al_2O_3) at the same reaction conditions. These results are in agreement with the high selectivity to ethylene achieved over MoVTeNb-M1 catalyst (with yield of ethylene of ca. 75%), with the high drop of the selectivity to ethylene observed over VOx/Al_2O_3 catalyst during the ethane ODH when the ethane conversion increases (and yield of ethylene up to 10%), or the intermediate behavior observed for NiSnOx catalysts (with yield of ethylene up to 30%).

To understand better these catalytic behaviors, microcalorimetry of adsorption of ethane or ethylene, infrared study at low temperature of adsorbed compounds (CO and ethylene) and operando IR study of ethylene and O_2 co-adsorption (in reaction conditions) were

considered. Both the microcalorimetry results and the infrared study at low temperature of adsorbed ethylene suggest that MoVTeNb-M1 shows the highest heat of adsorption for both ethane and ethylene (with ethylene interacting slightly stronger than ethane) on the surface of this catalyst and the higher interaction strength between ethylene and Lewis acid sites, respectively. However, VOx/Al_2O_3 and NiSnOx catalysts present a very low interaction with ethane or ethylene at low temperature.

The different catalytic behavior of these catalysts can be better explained from the comparison of ethylene oxidation results and the operando IR studies of ethylene and O_2 co-adsorption experiments. Thus, a fast desorption of ethylene is observed at higher temperatures over MoVTeNbO-M1 catalyst (without any additional IR signal) suggesting a nonexistence of reaction between ethylene and oxygen. In an opposite trend, NiSnOx and VOx/Al_2O_3 catalysts present several IR bands during ethylene/O_2 co-adsorption experiments (moderate temperatures) indicating the appearance of O-containing compounds, which can be transformed into carbon oxides at higher temperatures. The medium/low capacity of the NiSnOx active sites to oxidize ethylene is not due to a low over-oxidation activity of their sites but to the presence of many free Lewis sites not taking part in the ethylene oxidation reaction. In fact, a relatively high formation of oxygenated species, precursors of CO_x, over NiSnOx catalyst has been observed by IR. In contrast, the undesired high ethylene oxidation activity of the VOx/Al_2O_3 catalyst is mainly due to the fact that all active sites are involved in both ethane and ethylene oxidation with the non-selective oxidation path in ethylene deep oxidation.

According to the results obtained, the high stability of ethylene on MoVTeNb-M1 active sites is not due to a weak adsorption of ethylene but to the scarce ability of its active sites to activate ethylene. Although the results presented here suggest that the presence of V^{4+} species (majority in MoVTeNb-M1 and minority in VOx/Al_2O_3) improves the selectivity

to ethylene, it does not seem to be sufficient to explain the catalytic behavior of catalysts presenting the M1 phase. In fact, the results obtained for a supported vanadium-containing hexagonal tungsten bronzes (W-V-O/Al_2O_3 catalyst [62]), which mostly present V^{4+} species, show a catalytic behavior in ethane ODH better than that of VOx/Al_2O_3 but worse than MoVTeNb-M1. Thus, the catalytic performance of MoVTeNbO mixed oxides can be related to the presence of heptagonal channels in M1 structure (with similar size than the kinetic diameter of ethane/ethylene molecule, ca. 3.8 Å), in which the H-abstraction of ethane is carried out, in agreement to other authors [36, 39, 65, 66]. The low specificity to ethylene transformation of isolated V^{4+} species (probably in V-O-Mo pairs inside the heptagonal channels) can be a key factor for achieving high selectivity to ethylene.

Declaration of Competing Interest

The authors declare that they have no known competing financial interests or personal relationships that could have appeared to influence the work reported in this paper.

Acknowledgements

The authors would like to acknowledge the Ministerio de Ciencia, Innovación y Universidades of Spain (CRTl2018-099668-BC21, MAT2017-84118-C2-1-R and MAT2017-87500-P) and FEDER. Authors from ITQ also thank Project SEV-2016-0683 for supporting this research. A.A. acknowledges Severo Ochoa Excellence Program for his fellowship (BES-2017-080329).

References

1) J. Haber, "Oxidation of hydrocarbons", in: G. Ertl, H. Knoezinger, J. Weitkamp (Eds.), Handbook of Heterogeneous Catalysis, 4.6.2., Wiley-VCH (1997), pp. 2253-2274.

2) R.K. Grasselli, "Ammoxidation", in: G. Ertl, H. Knoezinger, J. Weitkamp (Eds.), Handbook of Heterogeneous Catalysis, 4.6.6, Wiley-VCH (1997) pp. -302, and references therein.

3) J. Haber, The concept of structure-sensitivity in catalysis by oxides, Stud. Surf. Sci. Catal. 48 (1989) 447-466]

4) J. Haber, Catalytic oxidation- State of the art and prospects, Stud. Surf. Sci. Catal. 72 (1992) 279-304.

5) J. Haber, Selectivity in Heterogeneous Catalytic Oxidation of Hydrocarbons, in Heterogeneous Hydrocarbon Oxidation, ACS Symp. Series 638 (1996) 20-34.

6) R.K. Grasselli, Site isolation and phase cooperation: Two important concepts in selective oxidation catalysis: A retrospective, Catal. Today 238 (2014) 10-27.

7) R.K. Grasselli, J.D. Burrington, D.J. Buttrey, P. DeSanto Jr., Cl.G. Lugmair, A F. Volpe Jr., T. Weingand, Multifunctionality of active centers in (amm)oxidation catalysts: from Bi–Mo–Ox to Mo–V–Nb–(Te;Sb)–Ox, Top. Catal. 23 (2003) 5-22.

8) R.K. Grasselli, Fundamental principles of selective heterogeneous oxidation catalysis, Top. Catal. 21 (2002) 79-88.

9) R.K. Grasselli, Advances and future trends in selective oxidation and ammoxidation catalysis, Catal. Today 49 (1999) 141-153.

10) E.G. Rightor, C.L. Tway, Global energy & emissions reduction potential of chemical process improvements, Catal. Today 258 (2015) 226–229.

11) Ch. Baroia, A. M. Gaffney, R. Fushimia, Process economics and safety considerations for the oxidative dehydrogenation of ethane using the M1 catalyst, Catal. Today 298 (2017) 138–144.

12) A.M. Gaffney, J.W. Sims, V. Martin, N.V. Duprez, K.J. Louthan, K. L. Roberts, Evaluation and analysis of ethylene production using oxidative Dehydrogenation, Catal. Today (2020) in press; https://doi.org/10.1016/j.cattod.2020.06.017

13) F. Cavani, N. Ballarini, A. Cericola, Oxidative dehydrogenation of ethane and propane: How far from commercial implementation? Catal. Today 127 (2007) 113-131.

14) C.A. Gärtner, A.C. van Veen, J.A. Lercher, Oxidative Dehydrogenation of Ethane: Common Principles and Mechanistic Aspects, ChemCatChem 5 (2013) 3196-3217.

15) J.T. Grant, J.M. Venegas, W.P. McDermott, I. Hermans, Aerobic Oxidations of Light Alkanes over Solid Metal Oxide Catalysts, Chem. Rev. 118 (2018) 2769-2815.

16) T. Blasco, J.M. López Nieto, Oxidative dehydrogenation of short chain alkanes on supported vanadium oxide catalysts. Appl Catal A Gen. 157 (1997) 117-142.

17) H.H. Kung, Oxidative dehydrogenation of light (C_2 to C_4) alkanes, Adv. Catal. 40 (1994) 1-38.

18) T. Blasco, A. Galli, J. M. López Nieto, F. Trifiro, Oxidative Dehydrogenation of Ethane and n-Butane on VOx/Al_2O_3 Catalysts, J. Catal. 169 (1997) 203-211.

19) K. Chen, A. T. Bell, E. Iglesia, The Relationship between the Electronic and Redox Properties of Dispersed Metal Oxides and Their Turnover Rates in Oxidative Dehydrogenation Reactions. J. Catal. 209 (2002) 35−42.

20) M.D. Argyle, K. Chen, A.T. Bell, E. Iglesia, Effect of Catalyst Structure on Oxidative Dehydrogenation of Ethane and Propane on Alumina-Supported Vanadia, J. Catal. 208 (2002) 139–149.

21) A. Dinse, R. Schomäcker, A. T. Bell, The role of lattice oxygen in the oxidative dehydrogenation of ethane on alumina-supported vanadium oxide, Phys. Chem. Chem. Phys. 11 (2009) 6119–6124.

22) B. Frank, R. Fortrie, Ch. Hess, R. Schlögl, R. Schomäcker, Reoxidation dynamics of highly dispersed VOx species supported on γ-alumina, Appl. Catal. A Gen. 353 (2009) 288–295.

23) H. Kim, G.A. Ferguson, L. Cheng, S.A. Zygmunt, P.C. Stair, L.A. Curtiss, Structure-Specific Reactivity of Alumina-Supported Monomeric Vanadium Oxide Species, J. Phys. Chem. C 116 (2012) 2927–2932.

24) a) E. Heracleous, A.A. Lemonidou, Ni–Nb–O mixed oxides as highly active and selective catalysts for ethene production via ethane oxidative dehydrogenation. Part I: Characterization and catalytic performance, J. Catal. 237 (2006) 162-174; b) E. Heracleous, A.A. Lemonidou, Ni–Nb–O mixed oxides as highly active and selective catalysts for ethene production via ethane oxidative dehydrogenation. Part II: Mechanistics aspects and kineting modeling, J. Catal. 237 (2006) 175-189.

25) (a) Liu, US Patent 6, 891,075, 2005; (b) Y. Liu, US Patent 7,227,049 A2 (2007); Assigned to Symyx Solutions Inc.

26) E. Heracleous, A.F. Lee, K. Wilson, A.A. Lemonidou, Investigation of Ni-based alumina-supported catalysts for the oxidative dehydrogenation of ethane to ethylene: structural characterization and reactivity studies, J. Catal. 231 (2005) 159-171.

27) E. Heracleous, A.A. Lemonidou, Ni–Me–O mixed metal oxides for the effective oxidative dehydrogenation of ethane to ethylene- Effect of promoting metal Me, J. Catal. 270 (2010) 67-75.

28) B. Solsona, P. Concepción, B. Demicol, S. Hernández, J.J. Delgado, J.J. Calvino, J.M. López Nieto, Selective oxidative dehydrogenation of ethane over SnO_2-promoted NiO catalysts, J. Catal. 295 (2012) 104-114.

29) H. Zhu, D.C. Rosenfeld, M. Harb, D.H. Anjum, M.N. Hedhili, S. Ould-Chikh, J.M. Basset, Ni−M−O (M = Sn, Ti, W) Catalysts Prepared by a Dry Mixing Method for Oxidative Dehydrogenation of Ethane, ACS Catal. 6 (2016) 2852–2866.

30) J. M. López Nieto, B. Solsona, R. K. Grasselli, P. Concepcion, Promoted NiO Catalysts for the Oxidative Dehydrogenation of Ethane, Top. Catal. 57 (2014) 1248–1255.

31) J.J. Varghese, S.H. Mushrif, Insights into the C−H Bond Activation on NiO Surfaces: The Role of Nickel and Oxygen Vacancies and of Low Valent Dopants on the Reactivity and Energetics, J. Phys. Chem. C 121 (2017) 17969−17981.

32) X. Lin, Y. Xi, J. Sun, Unraveling the Reaction Mechanism for Nickel-Catalyzed Oxidative Dehydrogenation of Ethane by DFT: The C−H Bond Activation Step and its Following Pathways, J. Phys. Chem. C 116 (2012) 3503−3516.

33) J.M. López Nieto, P. Botella, M.I. Vázquez, A. Dejoz, The selective oxidative dehydrogenation of ethane over hydrothermally synthesised MoVTeNb catalysts, Chem. Commun. (Camb) 7 (2002) 1906-7.

34) J.M. López Nieto, P. Botella, M.I. Vázquez, A. Dejoz, US Patent 7,319,179 B2 (2008); Assigned to CSIC and UPV.

35) P. Botella, E. García-González, A. Dejoz, J.M. López Nieto, M.I. Vázquez, J. González-Calbet, Selective oxidative dehydrogenation of ethane on MoVTeNbO mixed metal oxide catalysts, J. Catal. 225 (2004) 428-438.

36) a) T. Konya, T. Katou, T. Murayama, S. Ishikawa, M. Sadakane, D. Buttrey, W. Ueda, An orthorhombic Mo_3VO_x catalyst most active for oxidative dehydrogenation of ethane among related complex metal oxides, Catal. Sci. Technol. 3 (2013). 380-387; b) S. Ishikawa, D.i Kobayashi, T. Konya, S Ohmura, T. Murayama, N. Yasuda, M. Sadakane, W. Ueda, Redox Treatment of Orthorhombic $Mo_{29}V_{11}O_{112}$ and Relationships between Crystal Structure, Microporosity and Catalytic Performance for Selective Oxidation of Ethane, J. Phys. Chem. C 2015, 119, 7195−7206.

37) P. Kube, B. Frank, S. Wrabetz, J. Kröhnert, M. Hävecker, J. Velasco-Vélez, J. Noack, R. Schlögl, A. Trunschke, Functional Analysis of Catalysts for Lower Alkane Oxidation, ChemCatChem 9 (2017) 573-585.

38) P.J. Donaubauer, D.M. Melzer, K. Wanninger, G. Mestl, M. Sanchez-Sanchez, J.A. Lercher, O. Hinrichsen, Intrinsic kinetic model for oxidative dehydrogenation of ethane over MoVTeNb mixed metal oxides: A mechanistic approach, Chem. Eng. J. 383 (2020) 123195.

39) L. Annamalai, Y. Liu, S. Ezenwa, Y. Dang, S.L. Suib, P. Deshlahra, Influence of Tight Confinement on Selective Oxidative Dehydrogenation of Ethane on MoVTeNb Mixed Oxides, ACS Catal. 8 (2018) 7051−7067.

40) a) D. Melzer, G. Mestl, K. Wanninger, Y. Zhu, N. D. Browning, M. Sanchez-Sanchez, J.A. Lercher, Design and synthesis of highly active MoVTeNb oxides for ethane oxidative dehydrogenation, Nat. Commun. 10 (2019) 4012; b) D. Melzer, P. Xu, D. Hartmann, Y. Zhu, N.D. Browning, M. Sanchez-Sanchez, J.A. Lercher, Atomic-Scale

Determination of Active Facets on the MoVTeNb Oxide M1 Phase and Their Intrinsic Catalytic Activity for Ethane Oxidative Dehydrogenation, Angew. Chem. Int. Ed. 55 (2016) 8873-7.

41) M. Baca, A. Pigamo, J.L. Dubois, J.M.M. Millet, Catal. Commun. 6 (2005) 215–220.

42) S. Lwin, W. Diao, Ch.y Baroi, A.M. Gaffney, R.R. Fushimi, Characterization of MoVTeNbOx Catalysts during Oxidation Reactions Using In Situ/Operando Techniques: A Review, Catalysts 7 (2017) 109.

43) A.M. Gaffney, Q. An, W.A. Goddard III, W. Diao, M.V. Glazoff, Toward Concurrent Engineering of the M1-Based Catalytic Systems for Oxidative Dehydrogenation (ODH) of Alkanes, Top. Catal. 63 (2020) 1667–1681.

44) P. Concepcion, S. Hernandez, J.M. Lopez Nieto, On the nature of active sites in MoVTeO and MoVTeNbO catalysts: The influence of catalyst activation temperature, Appl. Catal. A Gen. 391 (2011) 92–101.

45) L. Koudelka, J. Pospísil, P. Mosner, L. Montagne, L. Delevoye, Structure and properties of potassium niobato-borophosphate glasses, J. Non-Cryst. Solids 354 (2008) 129-133.

46) D. Delgado, B. Solsona, R. Sanchis, E. Rodriguez-Castellon, J.M. López Nieto, Oxidative dehydrogenation of ethane on diluted or promoted nickel oxide catalysts: Influence of the promoter/diluter, Catal. Today 363 (2021) 27-35.

47) E. Aytan, B. Debnath, F. Kargar, Y. Barlas, M. M. Lacerda, J. X. Li, R. K. Lake, J. Shi, A. A. Balandin, Spi-phonon coupling in antiferromagnetic nickel oxide, Appl. Phys. Lett. 111 (2017) 252402.

48) a) M.A. Vuurmant, I. E. Wachs, In Situ Raman Spectroscopy of Alumina-Supported Metal Oxide Catalysts, J. Phys. Chem. 1992, 96, 5008-5016; b) Z. Wu, H.-S. Kim, P.C. Stair, S. Rugmini, S.D. Jackson, On the Structure of Vanadium Oxide Supported on Aluminas: UV and Visible Raman Spectroscopy, UV-Visible Diffuse Reflectance Spectroscopy, and Temperature-Programmed Reduction Studies, J. Phys. Chem. B 109 (2005) 2793-2800.

49) L.E. Briand, O.P. Tkachenko, M. Guraya, X. Gao, I. E. Wachs, W. Grünert, Surface-Analytical Studies of Supported Vanadium Oxide Monolayer Catalysts, J. Phys. Chem. B 108 (2004) 4823-4830

50) A. Massó Ramirez, F. Ivars-Barceló, J.M. Lopez Nieto, Optimizing Reflux Synthesis Method of Mo-V-Te-Nb mixed oxide Catalysts for Light Alkane Selective Oxidation, Catal. Today 356 (2020) 322–329.

51) K.I. Hadjiivanov, G.N. Vayssilov, Characterization of oxides surfaces and zeolites by carbon monoxide as IR probe molecule, Adv. Catal. 47 (2002) 307-511.

52) P. Concepción, K. Hajiivanov and H. Knözinger, Low-Temperature CO Adsorption on V-Containing Aluminophosphates: An FTIR Study, J. Catal. 184 (1999) 172-179.

53) a) G. Busca,V. Lorenzelli, G. Ramis, J. Saussey, J.C. Lavalley, FT-IR spectra of ethylene molecularly adsorbed on metal oxides, J. Mol. Struct. 267 (1992) 315-329; b) V. Sanchez Escribano, G. Busca, V. Lorenzelli, Fourier Transform Infrared Spectroscopic Studies of the Reactivity of Vanadia-Titania Catalysts toward Olefins. 2. Ethylene, J. Phys. Chem. 94 (1990) 8945-8948.

54) J. M. Lopez Nieto, J. Soler, P. Concepcion, J. Herguido, M. Menendez, J. Santamaria, Oxidative Dehydrogenation of Alkanes over V-based Catalysts: Influence of Redox Properties on Catalytic Performance, J. Catal. 185 (1999) 324–332.

55) D. Delgado, R. Sanchis, B. Solsona, P. Concepción, J.M. López Nieto, Influence of the Nature of the Promoter in NiO Catalysts on the Selectivity to Olefin During the Oxidative Dehydrogenation of Propane and Ethane, Top. Catal. 63 (2020) 1731-174.

56) F. Trifiró, I. Pasquon, Classification of oxidation catalysts according to the type of metal-oxygen bond, J. Catal. 12 (1968) 412-416

57) C. Doornkamp, M. Clement, X. Gao, G. Deo, I. E. Wachs, V. Ponec, The Oxygen Isotopic Exchange Reaction on Vanadium Oxide Catalysts, J. Catal. 185 (1999) 415–422.

58) K.R. William, G.E. Ewing, Infrared spectra and structure of ethane on NaCl (100), J. Phys. Chem. 99 (1995) 2186-2193.

59) G.C. Bond, K. Bruckman, Selective oxidation of o-xylene by monolayer V_2O_5–TiO_2 catalysts, Faraday Discuss. Chem. Soc. 72 (1981) 235-246.

60) X. Wang, B. Zhao, D. Jiang, Y. Xie, Monolayer dispersion of MoO_3, NiO and their precursors on γ-Al_2O_3, Appl. Catal. A Gen. 188 (1999) 201–209.

61) F. Trifiró, I. Pasquon, Classification of oxidation catalysts according to the type of metal oxygen bond, J. Catal. 12 (1968) 412-416.

62) S. Benomar, A. Chieregato, A. Masso, M.D. Soriano, J. A. Vidal-Moya, T. Blasco, R. Issaadi, J. M. López Nieto**,** Al_2O_3-Supported W-V-O bronzes catalysts for oxidative dehydrogenation of ethane, Catal. Sci Technol. 10 (2020) 8064-8076.

63) M. Hävecker, S. Wrabetz, J. Kröhnert, L.-I. Csepei, R.N. d'Alnoncourt, Y. V. Kolen'ko, F. Girgsdies, R. Schlögl, A. Trunschke, Surface chemistry of phase-pure M1 MoVTeNb oxide during operation in selective oxidation of propane to acrylic acid, J. Catal. 285 (2012) 48–60.

64) a) S. Ishikawa, X. Yi, T. Murayama, W. Ueda, Heptagonal channel micropore of orthorhombic Mo3VOx as catalysis field for the selective oxidation of ethane, Appl. Catal. A Gen. 474 (2014) 10–17; b) S. Ishikawa, W. Ueda, Microporous crystalline Mo–V mixed oxides for selective oxidations, Catal. Sci. Technol. 6 (2016) 617-629.

65) a) Sadakane, M.; Kodato, K.; Kuranishi, T.; Nodasaka, Y.; Sugawara, K.; Sakaguchi, N.; Nagai, T.; Matsui, Y.; Ueda, W. Molybdenum-vanadium-based molecular sieves with microchannels of seven-membered rings of corner-sharing metal oxide octahedra. Angew. Chem., Int. Ed. 47 (2008) 2493−2496; b) M. Sadakane, K. Kodato, N. Yasuda, S Ishikawa, W Ueda, Thermal Behavior, Crystal Structure, and Solid-State

Transformation of Orthorhombic Mo−V Oxide under Nitrogen Flow or in Air, ACS Omega 4 (2019) 13165−13171.

66) Y. Liu, L. Annamalai, P. Deshlahra, Effects of Lattice O Atom Coordination and Pore Confinement on Selectivity Limitations for Ethane Oxidative Dehydrogenation Catalyzed by Vanadium-Oxo Species, J. Phys. Chem. C 123 (2019) 28168−28191.

67) P. Concepcion, P. Botella, J.M. Lopez Nieto, Catalytic and FT-IR study on the reaction pathway for oxidation of propane and propylene on V- or Mo–V-based Catalysts, Appl. Catal. A Gen 278 (2004) 45–56.

68) R.N. d'Alnoncourt, L.-. Csepei, M. Hävecker, F. Girgsdies, M.E. Schuster, R. Schlögl, A. Trunschke, The reaction network in propane oxidation over phase-pure MoVTeNb M1 oxide catalysts, J. Catal. 311 (2014) 369–385.

69) P. Botella, J. M. Lopez Nieto, B. Solsona, A. Mifsud, F. Marquez, The Preparation, Characterization, and Catalytic Behavior of MoVTeNbO Catalysts Prepared by Hydrothermal Synthesis, J. Catal. 209 (2002) 445–455.

Table 1. Characteristics of catalysts.

Catalyst	**VOx/Al_2O_3**	**NiSnOx**	**MoVTeNbO-M1**
Composition (at. ratio)	V:Al = 5.5:94.5	Ni:Sn = 92:8	Mo:V:Te:Nb = 63:15:11:11
V or Ni (wt.%)	5.0	66.9	3.8
S_{BET} (m^2 g^{-1})	144	84	10
V- or Ni- surface content (10^{18} atoms m^{-2})	4.0 [a]	8.7 [b]	1.8
Heat-treatment	Air 550ºC (2h)	Air 500ºC (2h)	He 600ºC (2h)
XRD crystalline phases detected	γ-Al_2O_3	NiO	M1[c]
Other species present (Raman)	(VO_4) and (VO_4)$_n$ species	SnO_2 nanoparticles	-

a) Assuming that the cross-sectional area of a molecule of supported V_2O_5 is 0.201 nm^2 [ref. 59], a monolayer of vanadium oxide completely covering the surface of the support should need 4.98 x 10^{14} molec. V_2O_5 cm^{-2}.

b) Assuming that a monolayer of nickel oxide completely covering the surface of a support should need 9.7 x 10^{14} molec. NiO cm^{-2} [ref. 60]. Considering also a Ni/Sn atomic ratio of 92/8.

c) The presence of M2 (hexagonal bronze) as minority cannot be completely ruled out.

Table 2. Comparative results of microcalorimetic measurements.

Catalyst	**Hydrocarbon (HC)**	**Heat (J/g_{cat})**	**Adsorbed HC $\mu mol/g_{cat}$**	**Heat of adsorption (kJ/mol_{HC})**
MoVTeNb-M1	Ethane	1.546	48.6	32
MoVTeNb-M1	Ethylene	2.072	53.3	39
VOx/Al_2O_3	Ethane	1.334	110.7	12
VOx/Al_2O_3	Ethylene	1.184	122.9	10
NiSnOx	Ethane	2.004	154.1	13
NiSnOx	Ethylene	1.299	124.8	10

Table 3. Catalytic data in the ethane and ethylene oxidation on representative catalysts.[a]

Catalyst	VOx/Al_2O_3	NiSnOx	MoVTeNb-M1
Ethane ODH			
Reaction rate of ethane consumption ($mmol_{C2H6}\ g_{cat}^{-1}\ h^{-1}$)	0.68	17.6	2.29
Reaction rate of ethane consumption per active site ($mmol_{C2H6}\ g_{active\ site}^{-1}\ h^{-1}$)	13.7	26.3	60.3
Reaction rate of ethane consumption per surface area ($mmol_{C2H6}\ m^{-2}\ h^{-1}$)	0.09	0.31	6.0
Reaction rate of ethylene formation ($mmol_{C2H4}\ g_{cat}^{-1}\ h^{-1}$)	0.42	14.9	2.27
$n(C_2H_6)$ in ethylene formation [b]	0.80	0.52	0.88
$n(O_2)$ in ethylene formation [b]	0.15	0.26	0.22
Ethylene oxidation			
Reaction rate of ethylene consumption, ($mmol_{C2H4}\ g_{cat}^{-1}\ h^{-1}$)	1.76	3.71	0.17
Reaction rate of ethylene conversion per active site ($mmol_{C2H4}\ g_{active\ site}^{-1}\ h^{-1}$)	35.2	5.55	4.37
Rate per surface area ($mmol_{C2H4}\ m^{-2}\ h^{-1}$)	0.24	0.07	0.44
Relative reactivity ethylene/ethane	2.58	0.21	0.072

[a)] Reaction Temperature = 400ºC, Hydrocarbon/O_2/He = 5/5/90 (molar ratio); reaction rates were determined for conversions lower than 5%; [b] reaction order in the ethylene formation during the ethane oxidation $r = k\ P_{C2H6}^{n(C2H6)}\ P_{O2}^{n(O2)}$.

Caption to Figures

Fig. 1. TPR-H_2 results of catalysts: a) MoVTeNb-M1, b) NiSnOx; and c) VOx/Al_2O_3.

Fig. 2. IR spectra of CO adsorption at saturation coverage at -165 ºC on MoVTeNb-M1 (blue), NiSnOx (black) and VOx/Al_2O_3 (red). IR spectra have been normalized to sample weight and surface area.

Fig. 3. IR spectra of 43 mbar ethylene adsorbed at 25 ºC on MoVTeNb-M1 (blue), NiSnOx (black) and VOx/Al_2O_3 (red). IR band in the 1600-1630 cm^{-1} range corresponds to the ν(C=C).

Fig. 4. Variation of the selectivity to ethylene with the ethane conversion at 400 °C in the ODH of ethane. Catalysts: MoVTeNb(M1) (▲), NiSnOx (■), VOx/Al_2O_3 (●). Remaining reaction conditions in text.

Fig. 5. Variation of the selectivity to CO and CO_2 with the ethylene conversion, at 400 (●,▲, ■) and 450ºC (○, Δ, □,), during the oxidation of ethylene over MoVTeNb-M1 (▲, Δ), NiSnOx (■, □) and VOx/Al_2O_3 (●, ○) catalysts. Reaction conditions in the experimental section.

Fig. 6. Variation of the ethane and ethylene conversion with contact time, W/F, during the oxidation of ethane or ethylene over VOx/Al_2O_3 (a), NiSnOx (b) and MoVTeNb-M1 (c) catalysts. Reaction conditions: 400ºC, C_2/O_2/He: 5/5/90 molar ratio (for ethane or ethylene).

Fig. 7. Variation of the Oxidation of CO with reaction temperature over VOx/AL, NiSn-O and MoVTeNb(M1) catalysts. Reaction conditions: 0.5 mol% CO in synthetic air; 0.1 g of catalyst; total flow of 50 ml min^{-1}.

Fig.8. IR spectra of the co-adsorption ethylene and O_2 on MoVTeNb-M1 catalyst at increasing reaction temperatures: 25 ºC (red); 100 ºC (green); 150 ºC (blue);

200ºC (magenta); 250 ºC light grey (dark green). Cooling down at 250 ºC (highlighted orange line).

Fig. 9. IR spectra of the co-adsorption of ethylene and O_2 on NiSnOx (A) or VOx/Al_2O_3 (B) at increasing reaction temperatures: 25 ºC (red); 100 ºC (green); 150 ºC (blue); 200ºC (magenta); 250 ºC light grey (dark green). Cooling down at 250 ºC (highlighted orange line). In asterisk bands due to re-adsorption of ethylene.

Scheme 1. Reaction scheme for the oxidative dehydrogenation of ethane on: a) MoVTeNb-M1 or VOx/Al_2O_3; b) on NiSnOx.